

**SF₆ transport
processes in
troposphere**

P. K. Patra et al.

Transport mechanisms for synoptic, seasonal and interannual SF₆ variations in troposphere

P. K. Patra¹, M. Takigawa¹, G. S. Dutton², K. Uhse³, K. Ishijima¹, B. R. Lintner⁴, K. Miyazaki¹, and J. W. Elkins²

¹Frontier Research Center for Global Change, JAMSTEC, Yokohama 236 001, Japan

²NOAA Earth System Research Laboratory, Boulder, CO 80305, USA

³Umweltbundesamt - Federal Environment Agency, 63225 Langen, Germany

⁴Department of Atmospheric and Oceanic Sciences and Institute of Geophysics and Planetary Physics, University of California Los Angeles, Los Angeles, CA 90095-1565, USA

Received: 20 May 2008 – Accepted: 9 June 2008 – Published: 4 July 2008

Correspondence to: P. K. Patra (prabir@jamstec.go.jp)

Published by Copernicus Publications on behalf of the European Geosciences Union.

Title Page

Abstract

Introduction

Conclusions

References

Tables

Figures

◀

▶

◀

▶

Back

Close

Full Screen / Esc

Printer-friendly Version

Interactive Discussion



Abstract

We use an atmospheric general circulation model (AGCM) driven Chemistry-Transport Model (ACTM) to simulate the evolution of sulfur hexafluoride (SF_6) in the atmosphere. The model results are compared with continuous measurements at 6 sites over 71°N – 90°S . These comparisons demonstrate that the ACTM simulations lie within the measurement uncertainty over the analysis period (1999–2006) and capture salient features of synoptic, seasonal and interannual SF_6 variability. To understand transport timescales of SF_6 within the troposphere, transport times of air parcels from the surface to different regions of the troposphere (“age”) are estimated from a simulation of an idealized tracer. Monthly-mean, 2-box model exchange times (τ_{ex}) are calculated from both the observed and simulated SF_6 time series at the 6 observing sites and show favorable agreement, suggesting that the model adequately represents large-scale interhemispheric transport. The simulated SF_6 variability is further investigated through decomposition of the mixing ratio time-tendency into advective, convective, and vertical diffusive components. The transport component analysis illustrates the role of each process in SF_6 synoptic variability at the site level and provides insight into the seasonality of τ_{ex} .

1 Introduction

Sulfur hexafluoride (SF_6) represents a powerful tracer of atmospheric transport (Maiss et al., 1996). Emitted at the earth’s surface as a byproduct of industrial activity (primarily as a dielectric material in electrical switching equipment), SF_6 has no known production or loss in the troposphere or stratosphere (Ravishankara et al., 1993). Moreover, SF_6 emissions have no significant seasonal cycle. These characteristics render SF_6 ideal for illustrating the role of different transport processes (e.g. mean meridional transport, convection, vertical diffusion) on the tropospheric distribution of trace species. Like other minor tropospheric constituents, including ^{85}Kr and chlorofluorocar-

SF_6 transport processes in troposphere

P. K. Patra et al.

Title Page

Abstract

Introduction

Conclusions

References

Tables

Figures

◀

▶

◀

▶

Back

Close

Full Screen / Esc

Printer-friendly Version

Interactive Discussion



bons (CFCs) (Jacob et al., 1987; Prather et al., 1987), the potential for SF₆ to elucidate tropospheric transport mechanisms has led to its incorporation into model studies, especially as a metric for model intercomparison (e.g. Denning et al., 1996; Law et al., 2008).

5 Early applications of SF₆ to transport model diagnosis tended to focus on large-scale features such as the interhemispheric gradient. More recent observation-model comparisons of SF₆ (e.g. Peters et al., 2003; Gloor et al., 2007) have demonstrated that current generation transport models are able to resolve finer-scale latitudinal gradients as well as location-specific vertical distributions. The increased capacity of forward
10 transport models to replicate observed SF₆ can be attributed in large part to improvements in the models, including the treatment of diurnally varying planetary boundary layers (PBLs); the refinement of cumulus convective tracer mass transport, and the use of meteorological fields at higher spatial and temporal resolutions to drive advection (see, e.g. Rind et al., 2007 and references therein).

15 In the present study, we analyze the characteristics of SF₆ transport as simulated by the Center for Climate System Research/National Institute for Environmental Studies/Frontier Research Center for Global Change (CCSR/NIES/FRCGC) ACTM (hereafter, ATCM) on daily-to-interannual time scales and local-to-hemispheric space scales. The investigation of ATCM transport variability across multiple temporal and spatial
20 scales is crucial for assessing overall validity for applications such as source/sink inversion of atmospheric CO₂. For example, the inclusion of near-surface land region CO₂ measurement sites in CO₂ inversions may introduce uncertainties into estimated carbon fluxes because of deficiencies or errors in the representation or sampling of such sites in coarse resolution global transport models (Patra et al., 2006, 2008). In the
25 present CO₂ observational network, measurements at regular intervals (e.g. weekly) are mostly available near the surface (WDCGG, 2008). Because there are few sites where high frequency SF₆ data are available, we focus on the continuous observations of SF₆ from 6 sites, namely Point Barrow (BRW), Schauinsland (SCH), Niwot Ridge (NWR), Mauna Loa (MLO), Samoa (SMO) and South Pole (SPO). The present analy-

SF₆ transport processes in the troposphere

P. K. Patra et al.

Title Page

Abstract

Introduction

Conclusions

References

Tables

Figures

◀

▶

◀

▶

Back

Close

Full Screen / Esc

Printer-friendly Version

Interactive Discussion



SF₆ transport processes in the troposphere

P. K. Patra et al.

Title Page

Abstract

Introduction

Conclusions

References

Tables

Figures

◀

▶

◀

▶

Back

Close

Full Screen / Esc

Printer-friendly Version

Interactive Discussion



sis is motivated by a recent high-frequency model-observation intercomparison study, TransCom-4 (see Law et al., 2008; Patra et al., 2008) focusing on hourly and daily average CO₂ variations. An important conclusion of TransCom-4 is that the 25 participating models show some skill in simulating the observations, considering uncertainties or errors in CO₂ flux distribution and intensity. However, in that study, detailed analysis of SF₆ time series and transport characteristics was not performed, and the analysis was further restricted to the period of 2002–2003.

Apart from validating the ACTM's capacity to replicate the SF₆ records from the 6 observing sites, we further examine the roles of different transport processes in explaining variations of SF₆ as simulated by the ACTM. In particular, model simulations are used to analyze the vertical and horizontal aspects of tropospheric SF₆ transport. To quantify the vertical transport, we make use of an approach commonly applied to the stratosphere (see, e.g. Bischof et al., 1985; Hall and Plumb, 1994) to estimate the age of air in the troposphere. The horizontal transport, readily characterized in terms of an interhemispheric transport time (e.g. Jacob et al., 1987), is computed for both observed and simulated SF₆ data. A more detailed component analysis of ACTM-simulated SF₆ transport illustrates the transport pathways involved in both regional and large-scale atmospheric transport and how these pathways vary on different timescales.

2 Data and methodology

2.1 AGCM-based Chemistry Transport Model (ACTM)

The CCSR/NIES/FRCGC AGCM is nudged with NCEP/DOE AMIP-II Reanalysis (Kanamitsu et al., 2002; www.cpc.ncep.noaa.gov, path: products/wesley/reanalysis2) horizontal winds and temperature to drive the ACTM transport. This forward transport model has been adapted for simulations of greenhouse gases (CO₂, CH₄, N₂O, CFCs, SF₆ etc.) that have negligible production or chemical loss due to simple photochemistry in the troposphere and stratosphere. The ACTM is run in 'online' transport mode with

both the AGCM meteorology and chemical tracers simulated at the same integration timestep (~ 20 min). Although computationally expensive, running the ACTM in online mode offers some advantages over less demanding “offline” chemistry-transport models. Specifically, over the period of the analysis, the AGCM generates a detailed and consistent meteorology as represented by the grid- and subgrid-scale processes, surface processes (e.g. PBL height and mixing), above-PBL dynamics (e.g. convection) and interhemispheric gradients.

Another advantage of the online ACTM is that it can be run at finer spatial resolution than observed or reanalysis meteorology because it intrinsically generates a self-consistent meteorology at the model resolution (while offline models generally use interpolated meteorology). Because of the high computational cost, we use a relatively low resolution for this study, i.e. T42 truncation in the horizontal, or approximately $2.8^\circ \times 2.8^\circ$, and 32 vertical sigma-pressure layers up to ~ 50 km. While a comparison within TransCom-4 suggests that the higher horizontal resolution version (T106 truncation, $\sim 1.125^\circ \times 1.125^\circ$) performs better in simulating CO_2 at synoptic time scales compared to the T42 resolution version, no systematic differences can be identified between the two resolutions for simulating the CO_2 seasonal cycle or SF_6 interhemispheric gradient (Patra et al., 2008; Law et al., 2008).

The basic physical and dynamical features of the ACTM have been described in (Hasumi et al., 2004). Advective transport of moisture and tracers is obtained from a 4th order flux-form advection scheme using a monotonic Piecewise Parabolic Method (PPM) (Colella and Woodward, 1984) and a flux-form semi-Lagrangian scheme (Lin and Rood, 1996). Mass fluxes around the polar caps are calculated by using a semi-Lagrangian scheme in polar stereo projection. Subgrid-scale vertical fluxes of heat, moisture, and tracers are approximated using a non-local closure scheme based on Holtslag and Boville (1993) used in conjugation with the level 2 scheme of Mellor and Yamada (1974). The cumulus parameterization scheme is based on Arakawa and Schubert (1974) with some simplifications described in Numaguti et al. (1997); the updraft and downdraft of tracers by cumulus convection are calculated by using the

SF₆ transport processes in troposphere

P. K. Patra et al.

Title Page

Abstract

Introduction

Conclusions

References

Tables

Figures

◀

▶

◀

▶

Back

Close

Full Screen / Esc

Printer-friendly Version

Interactive Discussion



cloud mass flux estimated in the cumulus parameterization scheme.

Overall quality control of the ACTM transport in simulating SF₆ is assessed using recently published data (from Gloor et al., 2007) and is detailed in the supplemental information <http://www.atmos-chem-phys-discuss.net/8/12737/2008/acpd-8-12737-2008-supplement.pdf> available online (cf., Figs. S1 and S2). Note that ACTM performance in simulating spatiotemporal transport variations has been previously evaluated for CO₂, with behavior comparable to most other models and available observations (Law et al., 2008; Patra et al., 2008; Miyazaki et al., 2008).

2.2 Fluxes and data for SF₆, and curve fitting

We have simulated SF₆ for overall evaluation of regional and interhemispheric scale atmospheric tracer transport by the ACTM. The SF₆ emission distribution is taken from the Emission Database for Global Atmospheric Research (EDGAR) (Olivier and Berdowski, 2001), with the emission increase scaled to the SF₆ growth rate estimated from the Earth System Research Laboratory/National Oceanic and Atmospheric Administration, USA (ESRL/NOAA) observations (Geller et al., 1997). The atmospheric concentrations of SF₆ at daily time intervals are taken from the NOAA/ESRL halocarbon in situ network (Butler et al., 2004) and the Air Monitoring Network of Umweltbundesamt, Federal Environmental Agency, Germany (UBA/FEA). The geographic distribution of SF₆ emissions at the ACTM's horizontal resolution is displayed in Fig. 1 along with the locations of the 6 continuous measurement sites. Although the raw emission data are available at 1°×1°, there is considerable information loss at T42 resolution, e.g. emissions from the Korean peninsula and Japan are not easily distinguishable, and similarly high emissions from Europe and the United States are smeared out (referred to subsequently as spatial representation error).

A fitted curve and long-term trend for each daily average time series are derived using a Butterworth filter of order 16 (Nakazawa et al., 1997) with a cut-off length of 24 days. The time series are then decomposed into seasonal cycle (data or fitted curve-long-term trend), growth rate (time derivative of the long-term trend component)

SF₆ transport processes in troposphere

P. K. Patra et al.

Title Page

Abstract

Introduction

Conclusions

References

Tables

Figures

◀

▶

◀

▶

Back

Close

Full Screen / Esc

Printer-friendly Version

Interactive Discussion



and synoptic variation (data-fitted curve). Statistical assessments of modeled and observed data are determined using original values (without fitting) but excluding missing data.

2.3 “Age of air” tracer

5 The mean “age of air”, defined as the time required for an air parcel to transit from the earth’s surface to the layers above (Kida, 1983), is calculated as the difference between surface and upper air concentrations normalized by the concentration increase rate at the surface using a Green’s function method (Hall and Plumb, 1994). The Green’s function is estimated from the simulation of an idealized transport tracer with uniform
10 surface fluxes, linearly increasing trend, and no loss in the atmosphere.

2.4 Two-box model of interhemispheric (IH) exchange time (τ_{ex})

The interhemispheric exchange time (τ_{ex}) has been widely used for diagnosing large-scale model transport properties and has been previously estimated using both measured and modeled trace constituents (Jacob et al., 1987; Denning et al., 1996; Levin and Hesshaimer, 1996; Geller et al., 1997). τ_{ex} is computed from a simple
15 2-dimensional mass balance equation using the mean mixing ratios and growth rates in the Northern Hemisphere (NH) and Southern Hemisphere (SH) (see, e.g. Prather et al., 1987; Jacob et al., 1987):

$$\frac{dc_n}{dt} = 2\frac{E_n}{\alpha} - \frac{\Delta c_{n-s}}{\tau_{ex}} - \frac{c_n}{\tau_a} \quad (1)$$

$$20 \frac{dc_s}{dt} = 2\frac{E_s}{\alpha} + \frac{\Delta c_{n-s}}{\tau_{ex}} - \frac{c_s}{\tau_a} \quad (2)$$

Here, c_n and c_s are the average mixing ratios for the NH and SH, respectively; E_n and E_s are hemispheric total tracer emission; α is the emission-to-mixing ratio conversion

SF₆ transport processes in troposphere

P. K. Patra et al.

Title Page

Abstract

Introduction

Conclusions

References

Tables

Figures

◀

▶

◀

▶

Back

Close

Full Screen / Esc

Printer-friendly Version

Interactive Discussion



SF₆ transport processes in troposphere

P. K. Patra et al.

[Title Page](#)[Abstract](#)[Introduction](#)[Conclusions](#)[References](#)[Tables](#)[Figures](#)[◀](#)[▶](#)[◀](#)[▶](#)[Back](#)[Close](#)[Full Screen / Esc](#)[Printer-friendly Version](#)[Interactive Discussion](#)

factor; Δc_{n-s} is the north-south IH difference in tracer mixing ratio; and τ_a is the atmospheric lifetime of tracer. Since SF₆ has no known loss in the atmosphere up to about 50 km and its lifetime as estimated to be about 3200 years (Ravishankara et al., 1993), the last term in both equations can be neglected. By eliminating α from Eqs. (1) and (2), we can solve for τ_{ex} algebraically as

$$\tau_{ex} = \left[\Delta c_{n-s} \left(\frac{E_n}{E_s} + 1 \right) \right] / \left[\frac{E_n}{E_s} \frac{dc_s}{dt} - \frac{dc_n}{dt} \right] \quad (3)$$

All terms on the right hand side in Eq. (3) are estimated directly from either measured or modeled SF₆ time series. We used the fitted time series and monthly average values for calculation of monthly-mean τ_{ex} .

2.5 Separation of mass transport due to advection, convection and vertical diffusion

Tracer transport in the ACTM comprises numerical solution of the continuity equation that describes the mass conservation for a chemical tracer in the atmosphere:

$$\frac{\partial c}{\partial t} = -\nabla \cdot F + P - L \quad (4)$$

where ∇ is the 3-dimensional divergence operator and F is the tracer mass flux (includes both the direct advective effect and the parameterized diffusion term). P and L are production and loss in the atmosphere, respectively. L is neglected in the case of SF₆ for all model layers and P at all but the surface layer, where emissions are located. Thus the net tendency in c is caused entirely by the flux divergence term ($\nabla \cdot F$) associated with various transport processes; positive or negative in sign when a model grid gains or losses tracer mass. We decompose this flux divergence term into three components in this study: (1) advection by grid-scale air flow calculated from the flux-form transport scheme (Lin and Rood, 1996); (2) lifting through cumulus convection as parameterized by the Arakawa and Schubert (1974) scheme; and (3) vertical diffusion calculated using the turbulent closure method of Mellor and Yamada (1974).

These component tendencies are utilized to examine the impact of different transport mechanisms on the temporal evolution of SF₆.

3 Results and discussions

3.1 Model-observation comparison of SF₆ time series

5 Figure 2 compares observed and simulated SF₆ volume mixing ratios at the 6 continuous observing sites as well as the seasonal cycle and growth rate components of the time series. These results, together with the statistics presented in Table 1, indicate little disagreement between the observed and modeled latitudinal gradients, especially over the Pacific Ocean where the remote background sites BRW, MLO, and
10 SMO are located, and between the continental sites in North America (NWR) and Europe (SCH). In fact, differences between the simulated and observed time series fall within the measurement accuracy of 0.04 pptv. The amplitude and phasing of the high-frequency variability at all sites are also generally well captured. Some model-observation mismatches do occur, likely arising from spatial representation errors in
15 SF₆ emissions and ACTM transport as well as measurement quality issues.

Over the 1999–2006 period, some changes in observation-model agreement at high-frequencies are evident as instrumentation was altered. For example, marked improvements at SMO and MLO are evident around mid 2000 and mid 2002, respectively, following a change in electron capture detector (ECD). The observed synoptic or finer
20 time scale variability decreased significantly after the detector change, resulting in fluctuations more comparable to the simulations. Also, an ECD change in early 2004 clearly brings the model and observations into closer agreement at SPO, although the agreement deteriorates later in the record. At BRW the modeled concentrations were lower by about 0.05 pptv in 1999 and are higher by about 0.07 pptv in the
25 recent times compared to the observations. Such systematic differences, reflected in the BRW growth rate, may stem from errors in regional emission trends: while the rate of

SF₆ transport processes in troposphere

P. K. Patra et al.

Title Page

Abstract

Introduction

Conclusions

References

Tables

Figures

⏪

⏩

◀

▶

Back

Close

Full Screen / Esc

Printer-friendly Version

Interactive Discussion



emissions increase in our simulation is globally uniform, the actual trends are probably much larger in rapidly developing countries than in the developed countries. The overall agreement in the latitudinal gradient (Fig. 2, left column) between the simulations and measurements highlights realistic representation of the interhemispheric scale model transport in the ACTM.

The seasonal cycle and its interannual variability (IAV), as derived using the digital filtering method, are fairly well captured by the ACTM simulation at all background sites (Fig. 2g, j-l). By contrast, at the continental sites (NWR and SCH), there is no clear seasonality in SF₆ as the IAV is quite large. While the timings of SF₆ increases/decreases generally match between the observed and modeled results, their amplitudes are generally underestimated due to the ACTM's coarse horizontal resolution. We reiterate that the SF₆ emissions input to the ACTM do not have any seasonality (they vary linearly between years); thus the monthly or seasonal scale SF₆ fluctuations are driven entirely by atmospheric transport. Poorer agreement at the 2 continental sites compared to the 4 remote sites presumably results from site representation error within the ACTM's coarse horizontal resolution, i.e. the gridpoint at which the model is sampled may not adequately represent the conditions seen locally at the observing site. The degree to which this type of error contributes may further depend on how the features of local meteorology interact with nearby source emissions (with the latter generally negligible for remote observing sites).

We further illustrate the model-observation agreement of SF₆ synoptic variations at 5 sites (Fig. 3). Here, SPO is excluded because of low signal in the simulation, with variability ~0.005 pptv or less. As a measure of the phase similarity of modeled and observed SF₆, Pearson's correlation moment (r) values of observed and simulated daily mean SF₆ variability are significant at the 95% confidence interval only at SCH and SMO ($r > 0.28$, for number of data points > 600 in Student's 2-tailed test). Normalized standard deviations (NSDs; $= SD_{\text{observation}} / SD_{\text{model}}$; $= 1$ when modeled and observed variability amplitudes are equal regardless of the phase) are systematically > 1 at all sites, indicating smaller variability in the model than in the observations. In the daily-

SF₆ transport processes in the troposphere

P. K. Patra et al.

Title Page

Abstract

Introduction

Conclusions

References

Tables

Figures

⏪

⏩

◀

▶

Back

Close

Full Screen / Esc

Printer-friendly Version

Interactive Discussion



SF₆ transport processes in troposphere

P. K. Patra et al.

[Title Page](#)[Abstract](#)[Introduction](#)[Conclusions](#)[References](#)[Tables](#)[Figures](#)[⏪](#)[⏩](#)[◀](#)[▶](#)[Back](#)[Close](#)[Full Screen / Esc](#)[Printer-friendly Version](#)[Interactive Discussion](#)

averaged observed time series (thin lines), there are many positive and negative spikes lasting only for a day. Since the ACTM is likely incapable of simulating such sharp spikes because of the smoothed emissions, we also show 5-day (pentadal) running means (thick lines). Visually, the match between simulated and observed synoptic variability improves considerably for the pentadal time series, with both correlations and NSDs improved when 5-day moving window averages (MWAs; 1 average value for each 5-day block in the time series) are considered. By using 5-day MWAs we do not introduce spurious serial autocorrelations into the time series (as is the case for running means) although the length of the time series is reduced by factor of 0.2. Overall, the 5-day MWA correlations at all sites except BRW are found to be statistically significant at the 95% confidence interval ($r > 0.41$, for ~ 125 data points), while the NSDs are closer to 1 than those estimated for 1-day averages.

From the model-observation comparison, we conclude that the nudged ACTM at T42 horizontal resolution adequately simulates interhemispheric mixing ratio gradients, seasonal cycles at remote sites, and synoptic variations at 5-day time scales in SF₆. At the same time, we have also identified some limitations of the coarse resolution global models for simulating the highest-frequency fluctuations of SF₆. In the remainder of this study, we emphasize the simulated transport characteristics that are likely to be significant for SF₆ distributions on regional to global scales and compare some transport diagnostics estimated from observations and model simulations.

3.2 Mean “age of air” in troposphere

One of the ways to analyze model transport properties is the age distribution in troposphere, a concept widely applied to tracers in the stratosphere, where the tracer transport is much slower (age varies from 1–5 years; Bischof et al., 1985) relative to the troposphere. The mean age has been estimated using the idealized tracer simulation described in Sect. 2.3; latitude-height cross-sections of this timescale are depicted as filled contours in Fig. 4. The transport model reproduces the upper tropospheric mixing barrier around 30° in both hemispheres in most longitude bands and seasons

SF₆ transport processes in the troposphere

P. K. Patra et al.

Title Page

Abstract

Introduction

Conclusions

References

Tables

Figures

◀

▶

◀

▶

Back

Close

Full Screen / Esc

Printer-friendly Version

Interactive Discussion

(Erukhimova and Bowman, 2006). The upper tropospheric locations of the steepest meridional age gradients are coincident with the rapid change in zonal winds (black contours) corresponding to the equatorward edges of the subtropical jet streams. The steep gradient in the age-of-air in the subtropical upper troposphere may be associated with weak breaking of Rossby waves around the height of the 350 K potential isotherm (Postel and Hitchman, 1999), as the strong westerlies generally suppress Rossby wave breaking and thus slow mixing. The effect of this mixing barrier has also been shown in simulations of atmospheric CO₂ (Miyazaki et al., 2008).

For the longitude interval spanning the core of the Indian monsoon zone (Fig. 4b), the mixing barrier (defined by large age gradient) lies further north in NH summer because of the extensive cumulus convection near the Himalayan and Tibetan plateau region between 30–40° N. This region bears the signature of younger air at relatively higher altitudes (~150 mb or higher) in the NH compared to the SH at similar latitudes. Over the Pacific region (Fig. 4c, d) the tropical convective zone and upper tropospheric mixing barrier oscillates along with seasonal changes in solar insolation in the absence of heterogeneous orography. Note also that latitudinal gradients in isochrones are much steeper in the middle-upper troposphere (~400 mb and above) of the Indian monsoon zone in July (Fig. 4b) compared to January conditions or the mid-Pacific in either January or July (Fig. 4a, c and d).

Our estimation of the average age in the tropical upper troposphere, 20–30 days (at the 150 mb model layer; longitude: 87–80° W; latitude: 7–11° N; time: January–February), is within the range of the mean age of air (26±3 days) entering the tropical tropopause as estimated based from CO₂ measurements over Central America (latitude: <11° N; height: 14–18 km; time: January–February) (Park et al., 2007), although a more extensive data set is necessary to validate the age ranges implied by the modeled age distribution. The smallest vertical age gradients within the troposphere occur mainly where vertical potential temperature gradients (blue contours) are small, i.e. where there is prevailing conditions of dynamic or thermodynamic instability. The energy required for air parcels to crossing the isentropes is mainly supplied through

SF₆ transport processes in the troposphere

P. K. Patra et al.

diabatic heating/cooling processes such as convection. (The role of individual mechanisms in SF₆ transport is elaborated in Sect. 3.4). The sharp rise in age above the tropopause (potential temperature greater than 400 K and 380 K in the tropics and mid-latitude, respectively; note the unequal contour interval with height) is associated with the slower cross-isentropic transport under the strong thermal stratification of the lower stratosphere (with large increases of potential temperature with height). Thus, within the tropics, our age distribution calculation supports the conjecture of a vertical mixing barrier in the altitude range of 14 km and tropopause or potential temperature range ~360–390 K (Folkins et al., 1999), where the age increases from a few days below to about >100 days above.

3.3 Interhemispheric exchange time

Monthly-mean τ_{ex} estimated from both ACTM-simulated and observed SF₆ data appear in Fig. 5. For comparative purposes, hemispheric average mixing ratios were calculated from a few different combinations of the 4 northern and 2 southern hemispheric sites. For case 1 (light blue; Fig. 5a), all the sites in each hemisphere were used in averaging; the resulting τ_{ex} values are the largest because of the inclusion of non-background, higher concentration sites at SCH and NWR. Somewhat smaller values of τ_{ex} are evident for case 2 (black), in which only the SF₆ mixing ratios at the remote sites were used in averaging. For case 3, (blue) which used MLO and SMO concentrations as proxies for the NH and SH hemispheric averages, the lowest mean exchange times were obtained (resulting from the relatively small difference in mixing ratio between these close proximity sites) although the variability is clearly the largest. An additional case (4, black line; Fig. 5b), calculated from the ACTM simulation only using the average surface mixing ratio over all SH and NH gridpoints, produces similar τ_{ex} estimates to case 2, suggesting that SF₆ hemispheric averages consisting of BRW and MLO in the NH and SMO and SPO in SH are representative of the whole hemispheric averages.

Values of annual mean τ_{ex} , computed here for the various cases, are summarized

[Title Page](#)[Abstract](#)[Introduction](#)[Conclusions](#)[References](#)[Tables](#)[Figures](#)[◀](#)[▶](#)[◀](#)[▶](#)[Back](#)[Close](#)[Full Screen / Esc](#)[Printer-friendly Version](#)[Interactive Discussion](#)

SF₆ transport processes in the troposphere

P. K. Patra et al.

Title Page

Abstract

Introduction

Conclusions

References

Tables

Figures

◀

▶

◀

▶

Back

Close

Full Screen / Esc

Printer-friendly Version

Interactive Discussion

in Table 2 along with several estimates from prior studies. Both the observed and simulated results obtained in cases 1 and 2 compare well with the estimates of (Levin and Hesshaimer, 1996) and (Geller et al., 1997), considering the interannual variability in τ_{ex} . We point out that some differences between different studies may be tied to the selection of station sets for calculating the hemispheric average mixing ratios. The ACTM-derived τ_{ex} are also in the range of earlier SF₆ model-based estimates of 0.76–1.97 years obtained from multiple transport models (Denning et al., 1999). However, the more recent TransCom-4 intercomparison (Law et al., 2008) demonstrates much stricter agreement in SF₆ IH gradients. Specifically, 17 out of 20 global models examined produced IH gradients in the range of 0.21–0.29 pptv (0.24 pptv for the ACTM at T42) compared to an observed value of 0.23 pptv for the year 2002, implying less spread among the TransCom-4 τ_{ex} estimates. The closer agreement among models in the more recent intercomparison likely reflects improvements in forward transport modeling; moreover, all TransCom-4 models used analyzed meteorology to drive model transport, while in the earlier study modeling groups chose the meteorology divers independently (e.g. analyzed or GCM based winds). For case 4 as well as an analogous calculation using the total 3D mass distribution within the troposphere (case 5), annual-mean τ_{ex} values of 1.37 (case 4) and 0.7 (case 5) years are obtained. The case 5 estimate is within the range of 0.55–1.26 years (Denning et al., 1996) and more closely agrees with recent τ_{ex} model results of \sim 0.7–1.20 year (ref. Table 2). Based on the comparison shown in Table 2, a value of 0.7–0.8 year is appropriate for τ_{ex} corresponding to total hemispheric mass exchange, while a value of \sim 1.3 years is appropriate using surface-only mixing ratios of SF₆.

The monthly-mean τ_{ex} manifest pronounced seasonal cycles in all cases considered here. In particular, the seasonality is dominated by a semi-annual periodicity for the cases 4 and 5 (Fig. 5b). The primary and secondary maxima (slow IH exchange rates) are found during April and October, respectively, and minima during January and July (case 4). Timing of primary and secondary maxima altered in case 5. This seasonality is similar to that described in Lintner et al. (2004) but is distinct from the



seasonality shown in Levin and Hesshaimer (1996). Broadly, such seasonality can be understood in terms of the seasonal changes in the Hadley circulation and the meridional displacement of inter-tropical convergence zone (ITCZ) (Lintner et al., 2004), with the periods of strong Hadley-circulation related cross-equatorial transport associated with faster exchange of tracer mass. In fact, idealized model studies suggest that seasonal oscillation of the Hadley circulation is responsible for a significant portion (~78%) of IH mixing (Bowman and Cohen, 1997). A more complete picture of τ_{ex} seasonality in the ACTM is developed below.

3.4 Analysis of SF₆ transport pathways and seasonality in τ_{ex}

Tropospheric tracer transport in the ACTM consists of advection, convection, and vertical diffusion as described in Sect. 2.4. Figure 6 shows the latitude-pressure distributions of SF₆ mass transfer rates of each of these components. Generally, the advection term dominates in most parts of the troposphere, with the intensity maximized (≥ 1 pptm/mon) over 30° S–60° N, where the meridional gradient in SF₆ is the largest (black contours in Fig. 6a–d). The spatial gradient in SF₆ mixing ratio and wind speed are the main controlling factors of the advective transport. In a globally-averaged sense, cumulus convective transport is the next largest term, although it is principally localized to tropical and sub-tropical latitudes where it efficiently transfers mass from surface levels to the upper troposphere (see also Donner et al., 2007). Vertical diffusion plays the major role in delivering high, near-surface SF₆ mixing ratios over the source emission region (land areas between 20–60° N latitude; ref. Fig. 1) into the lower troposphere. Figure 6e–h and f–i indicate that the transport associated with convection is limited to the top of the Hadley cells, which has been suggested as a cause for the vertical mixing barrier in the tropical upper troposphere (see also Folkins et al., 1999).

In terms of the typical transport pathway connecting the source regions to remote portions of the troposphere, SF₆ emissions are initially mixed through vertical diffusion near the source regions (seen red in Fig. 6i–l). Except for the emission layer (model level #1), the model levels up to ~500 mb between roughly 30–60° N gain SF₆ through

SF₆ transport processes in the troposphere

P. K. Patra et al.

Title Page

Abstract

Introduction

Conclusions

References

Tables

Figures

◀

▶

◀

▶

Back

Close

Full Screen / Esc

Printer-friendly Version

Interactive Discussion



SF₆ transport processes in the troposphere

P. K. Patra et al.

Title Page

Abstract

Introduction

Conclusions

References

Tables

Figures

◀

▶

◀

▶

Back

Close

Full Screen / Esc

Printer-friendly Version

Interactive Discussion



vertical diffusion. From here, SF₆ is lofted deeper into the upper troposphere by convective transport from the lower troposphere (Fig. 6e–h). In regions of strong convection near the equator, the spacing between isentropes is reduced, which facilitates efficient and strong vertical mass transport in this part of the troposphere. Generally, increases to upper tropospheric SF₆ mixing ratios via convection are restricted to the north side of the upward branch of the Hadley circulation; to the south, upper tropospheric SF₆ values are reduced by convective uplift of low tropospheric air masses since the near-surface SH air is relatively deficient in SF₆. Negative values of the Eulerian mean pressure velocity (ω , in mb hr⁻¹), contoured in the right column of Fig. 6, correspond to large-scale ascent, with the strongest upward motion of the Hadley circulation located around 15° S (15° N) during boreal winter (summer). Upon its delivery to the middle and upper troposphere, SF₆ is advected longitudinally by strong zonal winds. Miyazaki et al. (2008) discuss detailed mechanisms of tropospheric CO₂ transport, with the results presented here supporting their conclusions. Relative to CO₂, the SF₆-based analysis is easier to visualize because of simpler emission statistics (i.e. well-defined source emission regions with no seasonality), and the simulated data can be readily validated against observations through simple transport diagnostics like τ_{ex} .

The Hadley circulation and its associated meridional winds advect SF₆ into the Tropics. The seasonality of τ_{ex} mirrors seasonalities seen in the convective and advective transport components of SF₆ near the equator. Figures 6e, g indicate that the maximum SF₆ transport to the upper troposphere through deep convection occurs near the equator, while Fig. 6a, c show upper tropospheric meridional spreading of SF₆ by advection across mixing ratio isopleths. This situation accounts for the faster tracer mass transport across the equator during January and July. On the other hand, during April and October, the regions of strong advective transport in the tropical upper troposphere do not cross the SF₆ mixing ratio isopleths. The apparent isolation of SF₆ transport on either side of the equator during the equinoctial seasons is consistent with the larger IH exchange times estimated from measured and simulated SF₆. Results

of a recent study by Aghedo et al. (2008) suggest that the seasonal asymmetry in τ_{ex} would be opposite, with the primary (secondary) maximum in October (April), for tracer emissions localized in the SH, although the reason for such sensitivity is unclear.

3.5 Contributions of transport pathways to SF₆ synoptic variations at surface sites

5 The transport components at the 5 continuous monitoring sites (excluding SPO) are presented in Fig. 7. It is clear that, depending on site location with respect to major emission regions and atmospheric transport regimes, the dominant mechanism(s) for SF₆ variability differs. The tendency components also exhibit distinct seasonality at some sites. At BRW, transport by advection (red) dominates in January when the winds are predominantly northerly. By contrast, during February–March, under the influence of stronger southerly flow, both advection and vertical diffusion (blue) are significant and generally of opposite phase, thereby attenuating the total synoptic-scale variability. At SCH, the antiphasing of synoptic SF₆ transport via advection and vertical diffusion is clearer. Advective and vertical diffusive transports are largest during the boreal winter, when PBL ventilation is weak, and smallest during the boreal summer, when PBL ventilation is strong: at this site (located at 1205 m altitude), the maximum PBL height simulated by the ACTM is typically 400 m during winter but as high as 1500 m during the summer. It is important to note that the simulated SF₆ at SCH was sampled at model level 3, even though the site is actually located on a mountain top, i.e. locally the earth's surface, which corresponds to model level 1 in the sigma-pressure coordinate. At the other continental site, NWR, the synoptic variability of advective transport is much larger than the vertical diffusive component; however, the magnitude of variability at NWR is several times smaller than that at SCH because of differences in SF₆ emission in their proximity (cf. Fig. 1; right column). At the remote MLO site, the synoptic variation in SF₆ is almost entirely driven by advection. Only at the remote marine site SMO is the convective transport (in cyan) of comparable magnitude to the advective transport at synoptic timescales. Interestingly, these two components are out of phase, with the tendencies changing sign seasonally; e.g. advection (con-

SF₆ transport processes in troposphere

P. K. Patra et al.

Title Page

Abstract

Introduction

Conclusions

References

Tables

Figures

◀

▶

◀

▶

Back

Close

Full Screen / Esc

Printer-friendly Version

Interactive Discussion



vection) shows positive (negative) tendencies during January–February and negative (positive) tendencies during March–September. These features can be understood from changes in SF₆ vertical structure and the Hadley circulation as seen in Fig. 6.

4 Conclusions

The CCSR/NIES/FRCGC AGCM-driven online transport model (ACTM) has been used for simulations of atmospheric SF₆. ACTM simulations of SF₆ are compared with the observed behavior at six continuous measurement sites, with mixing ratios increasing by about 1.6 and 1.8 pptv and at SPO (71° N) and BRW (90° S), respectively, between 1999 and 2006. Both the modeled and measured time series are decomposed into synoptic variations, seasonal cycles, and growth rates. The synoptic and seasonal variations of simulated and observed SF₆ data correlate statistically significantly at most sites during the analysis period. Thus ACTM can be utilized to study daily- to yearly- transport mechanisms in the troposphere.

An illustrative transport metric for the ACTM discussed here is the tropospheric “age of air”, which appears to conform to the available observation-based estimates of a few tens of days in the tropical upper troposphere. However, more observations are required for validating tropospheric age of air. Additionally, the interhemispheric exchange times (τ_{ex}), estimated using observed (~ 1.3 year) and modeled (~ 1.2 year) SF₆ mixing ratios, agree well with prior estimates based on earlier simulations/observations. While the value of the exchange time is somewhat dependent on the location of surface monitoring sites used in calculating hemispheric mean SF₆ mixing ratios, the combination of BRW and MLO in the NH and SMO and SPO in the SH reasonably represents their respective hemispheric mean surface mixing ratio for SF₆. The seasonality in τ_{ex} is shown to arise primarily from the seasonal migration of the zonal mean meridional advective transport across the equator. Stronger isolation of the NH (high SF₆ air) and the SH (low SF₆ air) occurs during boreal spring (April) and autumn (October), resulting in the slowest cross-equatorial exchange of tracer mass

SF₆ transport processes in the troposphere

P. K. Patra et al.

Title Page

Abstract

Introduction

Conclusions

References

Tables

Figures

◀

▶

◀

▶

Back

Close

Full Screen / Esc

Printer-friendly Version

Interactive Discussion



through the tropical upper troposphere.

From the tracer transport view perspective, vertical diffusion initially transfers SF₆ from its surface emission regions to the lower troposphere, after which tracer mass transport to the sub-tropical and tropical upper troposphere is accomplished by cumulus convective activity. The maximum mass exchange between the hemispheres occurs in the upper troposphere region via advection, indicating a shorter IH exchange time if the total hemispheric mass is considered rather than SF₆ surface-only values. The transport component analysis is further applied to understand the relative roles of three different transport processes at continental (near and far from source regions), remote (mountain and marine) sites.

Our study demonstrates that the ACTM adequately simulates the transport characteristics that are of relevance to inverse modeling or data assimilation of atmospheric trace species (CO₂, CH₄, N₂O etc.). In a follow-up study, we use the ACTM to perform a CO₂ inversion analysis of weekly measurements to estimate high-frequency regional CO₂ fluxes. Given the ACTM's capacity to replicate observed SF₆ without notable bias at regional and hemispheric scales, we anticipate lower bias in derived CO₂ fluxes at regional scale by inverse modeling of atmospheric-CO₂ and ACTM forward simulation.

Acknowledgements. This work is partly supported by the Grants-in-Aid for Creative Scientific Research (2005/17GS0203) of the Ministry of Education, Science, Sports and Culture, Japan. We appreciate the support of Takakiyo Nakazawa and Hajime Akimoto for this research, and we thank Bradley Hall for creating and maintaining the NOAA/ESRL 2006 SF₆ scale.

References

- Aghedo, A., Rast, S., and Schultz, M. G.: Sensitivity of tracer transport to model resolution, forcing data and tracer lifetime in the general circulation model ECHAM5, *Atmos. Chem. Phys. Discuss.*, 8, 137–160, 2008, <http://www.atmos-chem-phys-discuss.net/8/137/2008/>.
- Arakawa, A. and Schubert, W. H.: Interactions of cumulus cloud ensemble with the large-scale environment, Part I, *J. Atmos. Sci.*, 31, 671–701, 1974.

SF₆ transport processes in troposphere

P. K. Patra et al.

Title Page

Abstract

Introduction

Conclusions

References

Tables

Figures

◀

▶

◀

▶

Back

Close

Full Screen / Esc

Printer-friendly Version

Interactive Discussion



SF₆ transport processes in the troposphere

P. K. Patra et al.

Title Page

Abstract

Introduction

Conclusions

References

Tables

Figures

◀

▶

◀

▶

Back

Close

Full Screen / Esc

Printer-friendly Version

Interactive Discussion

- Bischof, W., Borchers, R., Fabian, P., and Krüger, B. C.: Increased concentration and vertical distribution of carbon dioxide in the stratosphere, *Nature*, 316, 708–710, 1985.
- Bowman, K. P. and Cohen, P.: Interhemispheric exchange by seasonal modulation of the Hadley circulation, *J. Atmos. Sci.*, 54, 2045–2059, 1997.
- 5 Butler, J. H., Daube, B. C., Dutton, G. S., Elkins, J. W., Hall, B. D., Hurst, D. F., King, D. B., Kline, E. S., Lafleur, B. G., Lind, J., Lovitz, S., Mondeel, D., Montzka, S. A., Moore, F. L., Nance, J. D., New, J. L., Romashkin, P. A., Scheffer, A., and Snible, W. J.: Halocarbons and Other Atmospheric Trace Species, Chapter 5 in: CMDL Summary Report No. 27, 2002–2003, NOAA/US Department of Commerce, edited by: Thompson, T. M., Boulder, USA, 115–135, 2004.
- 10 Colella, P. and Woodward, P. R.: The Piecewise Parabolic Method (PPM) for Gas-Dynamic Simulations, *J. Comput. Phys.*, 54, 174–201, 1984.
- Denning, A. S., Holzer, M., Gurney, K. R., Heimann, M., Law, R. M., Rayner, P. J., Fung, I. Y., Fan, S., Taguchi, S., Friedlingstein, P., Balkanski, Y., Maiss, M., and Levin, I.: Three-dimensional transport and concentration of SF₆: A model intercomparison study (Transcom 2), *Tellus*, 51B, 266–297, 1999.
- 15 Donner, L. J., Horowitz, L. W., Fiore, A. M., Seman, C. J., Blake, D. R., and Blake, N. J.: Transport of radon-222 and methyl iodide by deep convection in the GFDL Global Atmospheric Model AM2, *J. Geophys. Res.*, 112, D17303, doi:10.1029/2006JD007548, 2007.
- 20 Erukhimova, T. and Bowman, K. P.: Role of convection in global-scale transport in the troposphere, *J. Geophys. Res.*, 111, D03105, doi:10.1029/JD006006, 2006.
- Folkens, I., Lowenstein, M., Podolske, J., Oltmans, S., and Proffitt, M.: A barrier to vertical mixing at 14 km in the tropics: Evidence from ozonesondes and aircraft measurements, *J. Geophys. Res.*, 104, 22 095–22 102, 1999.
- 25 Geller, L. S., Elkins, J. W., Lobert, J. M., Clarke, A. D., Hurst, D. F., Butler, J. H., and Myers, R. C.: Tropospheric SF₆: Observed latitudinal distribution and trends, derived emissions and interhemispheric exchange time, *Geophys. Res. Lett.*, 24, 675–678, 1997.
- Gloor, M., Dlugokencky, E., Brenninkmeijer, C., Horowitz, L., Hurst, D. F., Dutton, G., Crevoisier, C., Machida, T., and Tans, P.: Three-dimensional SF₆ data and tropospheric transport simulations: Signals, modeling accuracy, and implications for inverse modeling, *J. Geophys. Res.*, 112, D15112, doi:10.1029/2006JD007973, 2007.
- 30 Hall, T. M. and Plumb, R. A.: Age as a diagnostic of stratospheric transport, *J. Geophys. Res.*, 99, 1059–1070, 1994.



SF₆ transport processes in the troposphere

P. K. Patra et al.

Title Page

Abstract

Introduction

Conclusions

References

Tables

Figures

◀

▶

◀

▶

Back

Close

Full Screen / Esc

Printer-friendly Version

Interactive Discussion



- Hasumi, H., Emori, S., Abe-Ouchi, A., et al.: K-1 Coupled GCM (MIROC) Description, Technical report, CCSR, Kashiwa, Chiba, Japan, 2004.
- Holslag, A. A. M. and Boville, B.: Local versus nonlocal boundary-layer diffusion in a global climate model, *J. Climate*, 6, 1825–1842, 1993.
- 5 Jacob, D. J., Prather, M. J., Wofsy, S. C., and McElroy, M. B.: Atmospheric distribution of ⁸⁵Kr simulated with a general circulation model, *J. Geophys. Res.*, 92, 6614–6626, 1987.
- Kanamitsu, M., Ebisuzaki, W., Woolen, J., Potter, J., and Fiorino, M.: NCEP/DOE AMIP-II Reanalysis (R-2), *Bull. Amer. Met. Soc.*, 83, 1631–1643, 2002.
- 10 Kida, H.: General circulation of air parcels and transport characteristics derived from a hemispheric GCM, Part 2, Very longterm motions of air parcels in the troposphere and stratosphere, *J. Meteor. Soc. Japan*, 61, 510–522, 1983.
- Law, R. M., Peters, W., Rödenbeck, C., et al.: TransCom model simulations of hourly atmospheric CO₂: experimental overview and diurnal cycle results for 2002, *Glob. Biogeochem. Cy.*, doi:10.1029/2007GB003050, in press, 2008.
- 15 Levin, I. and Hesshaimer, V.: Refining of atmospheric transport model entries by the globally observed passive tracer distributions of 85krypton and sulfur hexafluoride (SF₆), *J. Geophys. Res.*, 101, 16 745–16 756, 1996.
- Lin, S.-J. and Rood, R.: Multidimensional flux-form semi-Lagrangian transport schemes, *Mon. Weather Rev.*, 124, 2046–2070, 1996.
- 20 Lintner, B. R., Gilliland, A. B., and Fung, I. Y.: Mechanisms of convection-induced modulation of passive tracer interhemispheric transport interannual variability, *J. Geophys. Res.*, 109, D13102, doi:10.1029/2003JD004306, 2004.
- Maiss, M., Steele, L. P., Francey, R. J., Fraser, P. J., Langenfelds, R. L., Trivett, N. B. A., and Levin, I.: Sulfur hexafluoride – A powerful new atmospheric tracer, *Atmos. Environ.*, 30, 1621–1629, 1996.
- 25 Mellor, G. L. and Yamada, T.: A hierarchy of turbulence closure models for planetary boundary layers, *J. Atmos. Sci.*, 31, 1791–1806, 1974.
- Miyazaki, K., Patra, P. K., Takigawa, M., Iwasaki, T., and Nakazawa, T.: Global-scale transport of carbon dioxide in the troposphere; Part I. Lagrangian transport analysis, *J. Geophys. Res.*, doi:10.1029/2007JD009557, in press, 2008.
- 30 Nakazawa, T., Ishizawa, M., Higuchi, K., and Trivett, N. B. A.: Two curve fitting methods applied to CO₂ flask data, *Environmetrics*, 8, 197–218, 1997.
- Numaguti, A., Takahashi, M., Nakajima, T., and Sumi, A.: Development of CCSR/NIES Atmo-

- spheric General Circulation Model, CGER's Supercomput, Monogr. Rep., 3, 1–48, Tsukuba, Ibaraki, 1997.
- Olivier, J. G. J. and Berdowski, J. J. M.: Global emissions sources and sinks, in: The Climate System, edited by: Berdowski, J., Guicherit, R., and Heij, B. J., A. A. Balkema Publishers/Swets & Zeitlinger Publishers, Lisse, The Netherlands, ISBN 9058092550, 33–78, 2001.
- Park, S., Jiménez, R., Daube, B. C., Pfister, L., Conway, T. J., Gottlieb, E. W., Chow, V. Y., Curran, D. J., Matross, D. M., Bright, A., Atlas, E. L., Bui, T. P., Gao, R.-S., Twohy, C. H., and Wofsy, S. C.: The CO₂ tracer clock for the Tropical Tropopause Layer, Atmos. Chem. Phys., 7, 3989–4000, 2007,
<http://www.atmos-chem-phys.net/7/3989/2007/>.
- Patra, P. K., Gurney, K. R., Denning, A. S., Maksyutov, S., Nakazawa, T., et al.: Sensitivity of inverse estimation of annual mean CO₂ sources and sinks to ocean – only sites versus all-sites observational networks, Geophys. Res. Lett., 33, L05814, doi:10.1029/2005GL25403, 2006.
- Patra, P. K., Law, R. M., Peters, W., Rödenbeck, C., Takigawa, M., et al.: TransCom model simulations of hourly atmospheric CO₂: analysis of synoptic scale variations for the period 2002–2003, Glob. Biogeochem. Cy., doi:10.1029/2007GB003081, 2008.
- Postel, G. A. and Hitchman, M. H.: climatology of Rossby wave breaking along the subtropical tropopause, J. Atmos. Sci., 56, 359–373, 1999.
- Prather, M., McElroy, M., Wofsy, S., Russell, G., and Rind, D.: Chemistry of the Global Troposphere: Fluorocarbons as Tracers of Air Motion, J. Geophys. Res., 92, 6579–6613, 1987.
- Ravishankara, A. R., Solomon, S., Turnipseed, A. A., and Warren, R. F.: Atmospheric lifetimes of long-lived halogenated species, Science, 259, 194–199, 1993.
- Rind, D., Lerner, J., Jonas, J., and McLinden, C.: Effects of resolution and model physics on tracer transports in the NASA Goddard Institute for Space Studies general circulation models, J. Geophys. Res., 112, D09315, doi:10.1029/2006JD007476, 2007.
- Uhse, K., Meinhardt, F., and Ries, L.: Atmospheric SF₆ hourly concentration data, Schauinsland, in World Data Centre for Greenhouse Gases, Japan Meteorological Agency, Tokyo, (<http://gaw.kishou.go.jp/wdceg.html>), 2006.
- WDCGG: WMO World Data Centre for Greenhouse Gases, Japan Meteorological Agency, Tokyo (data available at <http://gaw.kishou.go.jp>), 2008.

SF₆ transport processes in the troposphere

P. K. Patra et al.

Title Page

Abstract

Introduction

Conclusions

References

Tables

Figures

◀

▶

◀

▶

Back

Close

Full Screen / Esc

Printer-friendly Version

Interactive Discussion



SF₆ transport processes in troposphere

P. K. Patra et al.

Table 1. Statistics of model-observation comparison of SF₆; average difference in daily concentrations (Diff.; observation–model), 1- σ standard deviation (SD), and number of observations (N) after taking into account the missing data for two different analysis time periods are given. Note the accuracy in continuous SF₆ measurements is about 0.04 pptv.

Site details				Period: Jan'99 – Dec'06			Period: Jan'03 – Dec'06		
Name	Location		Hgt	Diff. (pptv)	SD	N	Diff. (pptv)	SD	N
	Lat	Lon							
BRW	71.3° N	156.6° W	11 m	-0.0059	0.045	2612	-0.036	0.051	1334
NWR	40.0° N	105.6° W	3526 m	-0.015	0.073	1564	-0.025	0.077	898
SCH	47.9° N	7.9° E	1205 m	-0.0085	0.373	1737	+0.0034	0.389	1020
MLO	19.5° N	155.6° W	3397 m	+0.014	0.086	2294	-0.022	0.056	1402
SMO	14.2° S	170.6° W	42 m	+0.017	0.068	2486	+0.00031	0.034	1284
SPO	90.0° S	24.8° W	2810 m	+0.014	0.048	2541	-0.0077	0.043	1335

Title Page

Abstract

Introduction

Conclusions

References

Tables

Figures

◀

▶

◀

▶

Back

Close

Full Screen / Esc

Printer-friendly Version

Interactive Discussion

SF₆ transport processes in troposphere

P. K. Patra et al.

Table 2. Comparison of τ_{ex} (in year) between the model- and observation-based estimates found here and previously published estimates using SF₆ (LH96: Levin and Hesshaimer; LG97: Geller et al.; SD96: Denning et al.; BL04: Lintner et al.; DR07: Rind et al. [horizontal resolution: 3.2×2.5°]; AA08: Aghedo et al. [ERA-40 case]). For the results obtained here, error values corresponding to one standard deviation (1σ) are given, with σ calculated from annual mean values for the period 2001–2005, indicating the amplitude of interannual variability in τ_{ex} . The results obtained from multi-model transport are given as “range”.

τ_{ex} Estimation Method	ACTM Based Mean±1 σ	Observ. Based Mean±1 σ	LH96 Mean	LG97 Mean	SD96 Range	BL04 Range	DR07 Range	AA08 Mean
Site based estimates								
Case 1	1.75±0.03	1.86±0.16	1.50	1.30				
Case 2	1.21±0.01	1.33±0.18						
Case 3	1.07±0.40	0.99±0.31						
Whole Hemisphere Based Estimates								
Case 4	1.37±0.04				0.76–1.97			
Case 5	0.70±0.01				0.55–1.26	0.80–1.2	0.78–1.02	0.70

[Title Page](#)
[Abstract](#)
[Introduction](#)
[Conclusions](#)
[References](#)
[Tables](#)
[Figures](#)
[⏪](#)
[⏩](#)
[◀](#)
[▶](#)
[Back](#)
[Close](#)
[Full Screen / Esc](#)
[Printer-friendly Version](#)
[Interactive Discussion](#)


SF₆ transport processes in troposphere

P. K. Patra et al.

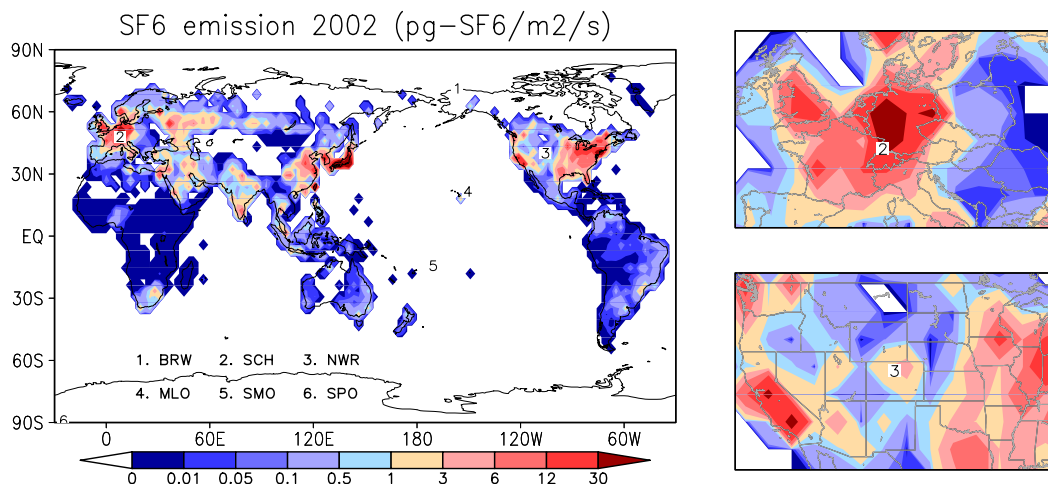


Fig. 1. Distribution of SF₆ emission (left column; in pg-SF₆ m⁻² s⁻¹; 1 pg=10⁻¹²g) at T42 resolution ($\sim 2.8^\circ \times 2.8^\circ$ latitude-longitude), with an annual total emission of 8.8×10^9 g-SF₆ yr⁻¹ for the year 2002. The measurement site locations are marked as numbers (1–6), with abbreviated names given at bottom-left (see Table 1 for location details). The MLO marker appears to the northeast of the site so that the island and emission grid are visible. In the right column are magnified views of the SF₆ emissions around the two continental sites (NWR and SCH).

Title Page

Abstract

Introduction

Conclusions

References

Tables

Figures

◀

▶

◀

▶

Back

Close

Full Screen / Esc

Printer-friendly Version

Interactive Discussion



SF₆ transport processes in troposphere

P. K. Patra et al.

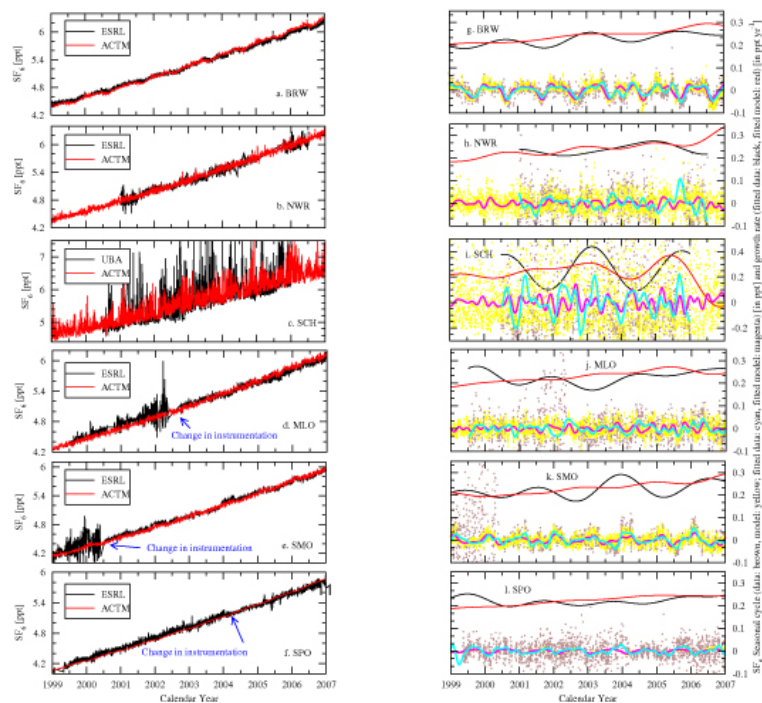


Fig. 2. Comparisons of observed and modeled SF₆ mixing ratio (in pptv; volume mixing ratio; ppt=parts per trillion) at 6 sites with continuous observations ((a–f), left column; daily averages, prepared from hourly data, are illustrated here; source: Butler et al. (2004), available online at <ftp.cmdl.noaa.gov>, path: /hats/sf6/insituGCs/CATS; Uhse et al. (2006), available online at <http://gaw.kishou.go.jp/wdcgg>). Some changes in measurement instrumentation during the period of comparison are indicated in blue text (see Sect. 3.1 for details). Panels appearing in the right column (g–i) show time series decomposed into seasonal cycle and growth rate components at each site (line colours are identified in the right axis title) using the digital filtering technique described in Sect. 2.2.

Title Page

Abstract

Introduction

Conclusions

References

Tables

Figures

◀

▶

◀

▶

Back

Close

Full Screen / Esc

Printer-friendly Version

Interactive Discussion



SF₆ transport processes in troposphere

P. K. Patra et al.

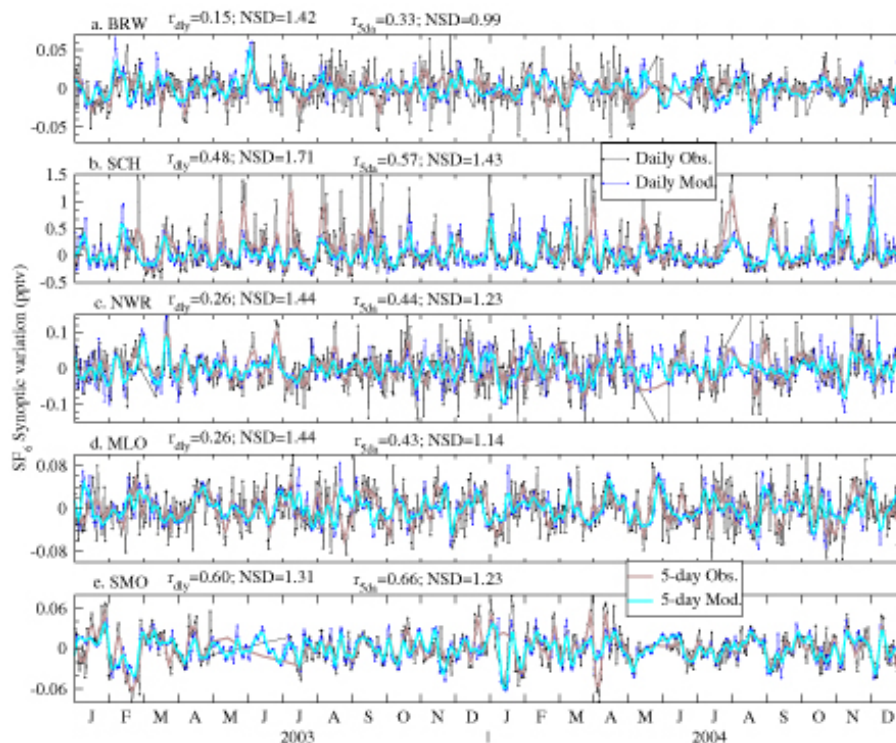


Fig. 3. Synoptic variations in SF₆ at 5 sites (excluding SPO, see Sect. 3.1 for details), derived by subtracting the fitted curve from daily mean values for both models and observations. Daily- and 5-day running means are shown as thin and thick lines, respectively, and the correlation coefficients (r) and normalized standard deviations (NSDs) are given in the panel title for each site. Note the variable y-axis scales in each panel.

Title Page

Abstract

Introduction

Conclusions

References

Tables

Figures

◀

▶

◀

▶

Back

Close

Full Screen / Esc

Printer-friendly Version

Interactive Discussion



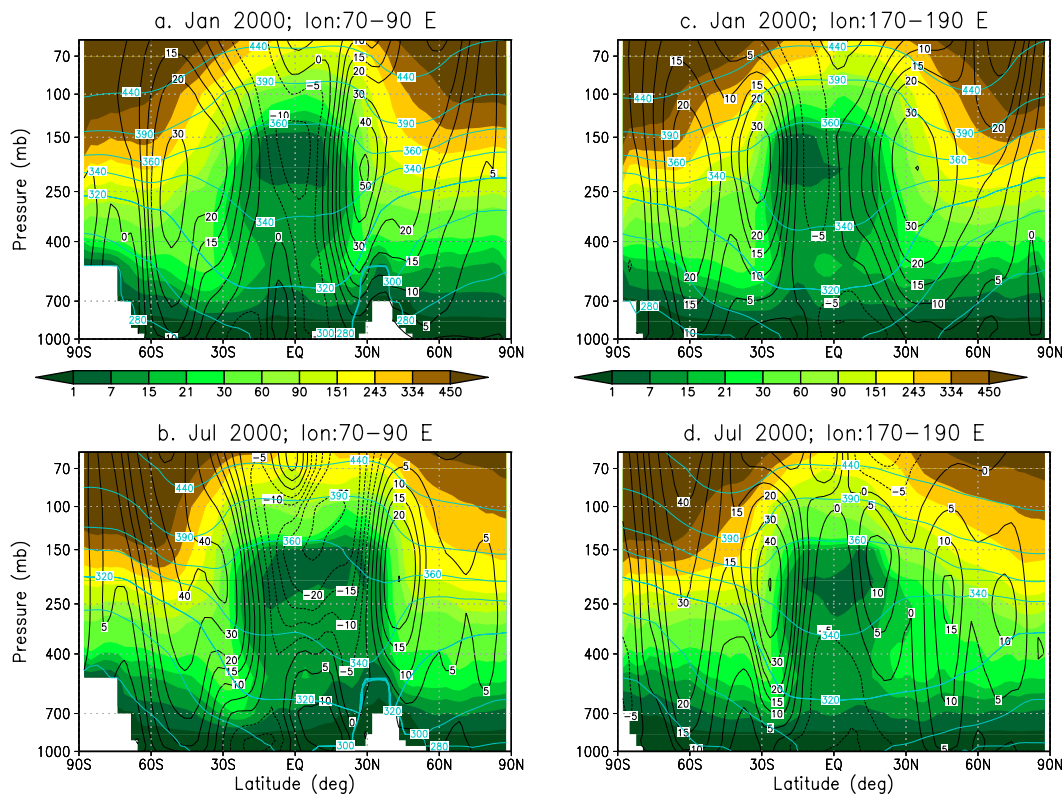


Fig. 4. Latitude-pressure cross-sections of mean age of air (in days) distribution in the troposphere during the boreal winter and summer of year 2000 (shaded). The contour line shows zonal wind speed (black contour, levels: -20 to 20 at an interval of 5 m s^{-1} , and 30 and 40 m s^{-1}) and potential temperature (blue contour, levels: 280 , 300 , 320 , 340 , 360 , 390 , 440 K) as simulated by the nudged ACTM run. Longitudinal averages are taken along the center of the Indian monsoon zone (left column) and the central Pacific (right column).

Title Page

Abstract

Introduction

Conclusions

References

Tables

Figures

◀

▶

◀

▶

Back

Close

Full Screen / Esc

Printer-friendly Version

Interactive Discussion



SF₆ transport processes in troposphere

P. K. Patra et al.

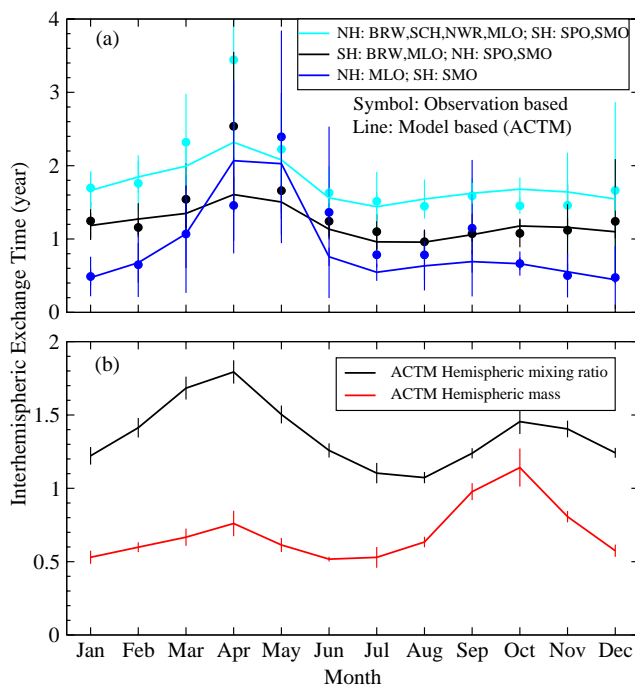


Fig. 5. Climatological average monthly-mean inter-hemispheric exchange time as estimated from SF₆ model simulation (line) and observations (symbol) at 6 sites and their three combinations to calculate hemispheric mean concentrations (top; panel (a)). Bottom panel (b) shows exchange times estimated using model based the hemispheric mean mixing ratio at the surface and total mass in the troposphere (surface to 100 mb).

[Title Page](#)[Abstract](#)[Introduction](#)[Conclusions](#)[References](#)[Tables](#)[Figures](#)[◀](#)[▶](#)[◀](#)[▶](#)[Back](#)[Close](#)[Full Screen / Esc](#)[Printer-friendly Version](#)[Interactive Discussion](#)

SF₆ transport processes in troposphere

P. K. Patra et al.

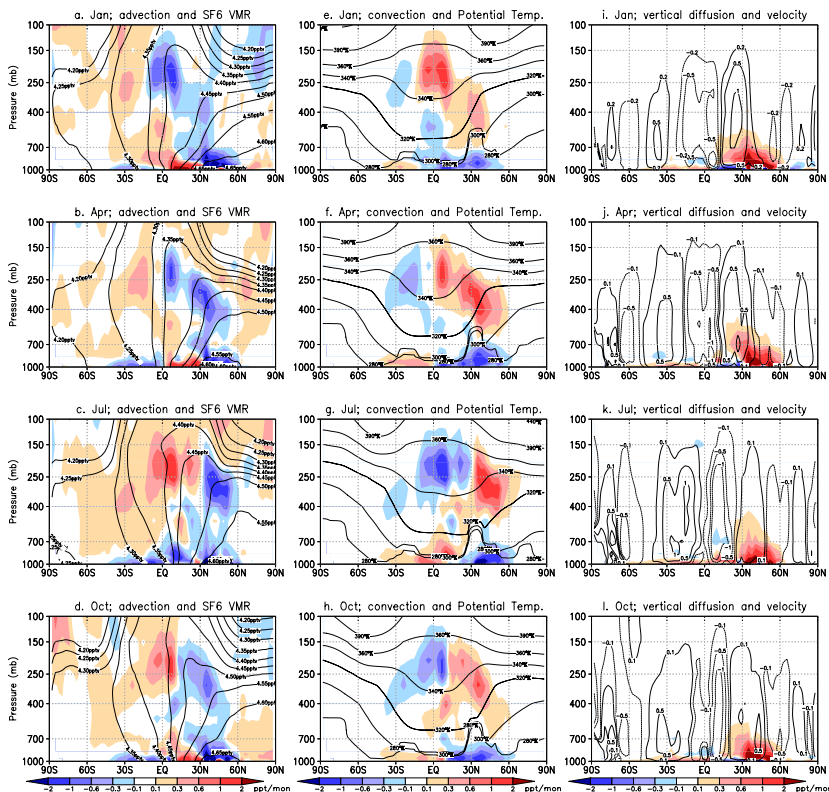


Fig. 6. Monthly and zonal average distributions of component SF₆ mass mixing ratio tendencies (in pptm month⁻¹) as modeled in the ACTM; panels **(a–d)** (left column): transport by grid-scale advection, **(e–h)** (middle column): convective transport, **(i–l)** (right column): vertical transport by diffusion (shaded). The black contours shown denote SF₆ mixing ratio (**a–d**; unit pptv); potential temperature (**e–h**; unit K); and vertical velocity (**(i–l)** unit: mb hr⁻¹). These contours are provided for interpreting relationships between the meteorological conditions and transport components as discussed in Sect. 3.4.

Title Page

Abstract

Introduction

Conclusions

References

Tables

Figures

◀

▶

◀

▶

Back

Close

Full Screen / Esc

Printer-friendly Version

Interactive Discussion



SF₆ transport processes in troposphere

P. K. Patra et al.

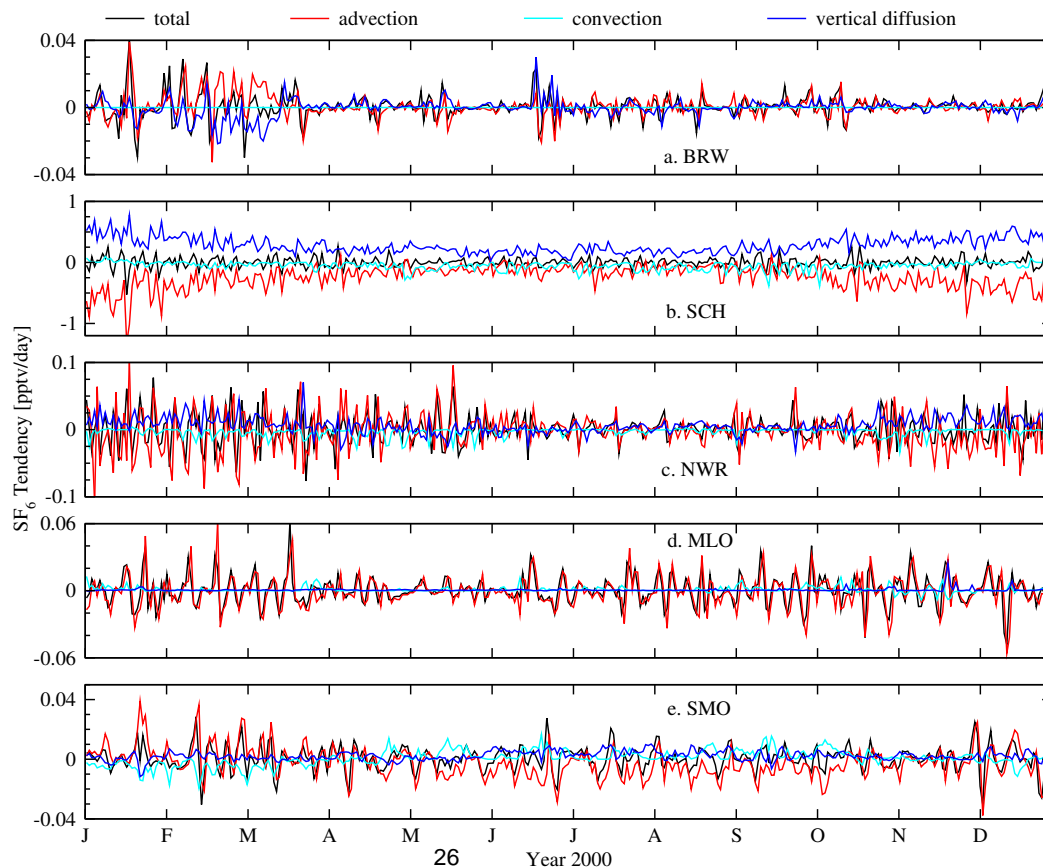


Fig. 7. Tendencies (in pptv/day) of modeled SF₆ mixing ratio and the three transport components at 5 sites. Averages are taken over 5 model grids (nearest sampling grid +4 around it) in order to reduce high frequency variations. The legend at the top for identifies each line.

[Title Page](#)[Abstract](#)[Introduction](#)[Conclusions](#)[References](#)[Tables](#)[Figures](#)[◀](#)[▶](#)[◀](#)[▶](#)[Back](#)[Close](#)[Full Screen / Esc](#)[Printer-friendly Version](#)[Interactive Discussion](#)